



Article

New Eco-Friendly, Biocompatible, Bactericidal, Fungicidal and Anticancer-Activity-Exhibiting Nanocomposites Based on Bimetallic $\text{TiO}_2@\text{Cr}_2\text{O}_3$ Nanoparticle Core and Biopolymer Shells

Mohamed S. Hasanin ^{1,*}, Yasser Elhenawy ^{2,3,4}, Shereen M. S. Abdel-Hamid ⁵, Yasser Fouad ⁶, Toderăș Monica ^{7,*}, O. A. Al-Qabandi ⁸, Miroslawa El Fray ⁹ and Mohamed Bassyouni ^{4,10,11}

- ¹ Department of Cellulose and Paper, National Research Centre, Dokki, Cairo 12622, Egypt
² Department of Mechanical Power Engineering, Faculty of Engineering, Port Said University, Port Said 42526, Egypt; dr_yasser@eng.psu.edu.eg
³ School of Chemical and Metallurgical Engineering, University of the Witwatersrand, 1 Jan Smuts Avenue, Johannesburg 2000, South Africa
⁴ Center of Excellence in Membrane-Based Water Desalination Technology for Testing and Characterization (CEMTC), Port Said University, Port Said 42526, Egypt; m.bassyouni@eng.psu.edu.eg
⁵ Egyptian Academy for Engineering and Advanced Technology (EA&EAT) Affiliated to Ministry of Military Production, Department of Chemical Engineering, Km# 3 Cairo-Belbeis Desert Road, Cairo 3066, Egypt; shereenahmed@eaeat.edu.eg
⁶ Department of Applied Mechanical Engineering, College of Applied Engineering, Muzahimiyah Branch, King Saud University, P.O. Box 800, Riyadh 11421, Saudi Arabia; yfouad@ksu.edu.sa
⁷ Faculty of Sciences, Oradea University St. No. 1, 410087 Oradea, Romania
⁸ School of Engineering and Technology, Chemical Engineering Department, American University of Middle East, 250 St., Block 6, Building 1, Egaila 54200, Kuwait; osamah.alqabandi@aum.edu.kw
⁹ Department of Polymer and Biomaterials Science, West Pomeranian University of Technology in Szczecin, Al. Piastow 45, 70-311 Szczecin, Poland; mirfray@zut.edu.pl
¹⁰ Department of Chemical Engineering, Faculty of Engineering, Port Said University, Port Said 42526, Egypt
¹¹ Department of Chemical Engineering, Faculty of Engineering, East Port Said University of Technology, North Sinai 45632, Egypt
* Correspondence: sido_sci@yahoo.com (M.S.H.); monicatoderas@gmail.com (T.M.)



Citation: Hasanin, M.S.; Elhenawy, Y.; Abdel-Hamid, S.M.S.; Fouad, Y.; Monica, T.; Al-Qabandi, O.A.; El Fray, M.; Bassyouni, M. New Eco-Friendly, Biocompatible, Bactericidal, Fungicidal and Anticancer-Activity-Exhibiting Nanocomposites Based on Bimetallic $\text{TiO}_2@\text{Cr}_2\text{O}_3$ Nanoparticle Core and Biopolymer Shells. *J. Compos. Sci.* **2023**, *7*, 426. <https://doi.org/10.3390/jcs7100426>

Academic Editor: Francesco Tornabene

Received: 15 August 2023

Revised: 26 September 2023

Accepted: 4 October 2023

Published: 10 October 2023



Copyright: © 2023 by the authors. Licensee MDPI, Basel, Switzerland. This article is an open access article distributed under the terms and conditions of the Creative Commons Attribution (CC BY) license (<https://creativecommons.org/licenses/by/4.0/>).

Abstract: Nanoparticles have attracted substantial attention for their diverse range of applications, particularly in biomedicine applications and drug delivery, owing to their unique properties. However, their tiny size facilitates easy cellular entry, which can also lead to interactions with cellular components, potentially resulting in toxicity and undesirable effects. In this study, a novel nanocomposite formulation was developed using biopolymers, specifically ethylcellulose and collagen, as capping and stabilizing agents to create bimetallic nanoparticles including $\text{TiO}_2@\text{Cr}_2\text{O}_3$ nanoparticles. Physicochemical and morphological analyses were carried out to validate the formulation's structure. The obtained characteristics emphasized the presence of a nanostructure involving bimetallic nanoparticles. This formulation exhibited excellent biological activity, including high biocompatibility with Vero and WI38 cells at concentrations of 40.4 and 52 $\mu\text{g}/\text{mL}$, respectively, as well as effective anticancer activity with significant selectivity. The IC₅₀ values were determined to be 19 and 22 $\mu\text{g}/\text{mL}$ for MCF7 and A549 cells, respectively. The antimicrobial assessment revealed the highest MIC value for *A. niger* at 50 $\mu\text{g}/\text{mL}$, while the lowest MIC value was observed for Gram-positive bacteria at 3.12 $\mu\text{g}/\text{mL}$. Additionally, the nanocomposite demonstrated antioxidant activity at a low concentration of 1.5 $\mu\text{g}/\text{mL}$.

Keywords: nanocomposite; biopolymer; glycogen; ethylcellulose; biocompatibility; bimetallic nanoparticles; antimicrobial activity

1. Introduction

Cancer is a disease that takes place when somebody's cells grow up fast and spread in an uncontrolled way to other body regions. It is recognized as the second global cause of death according to the World Health Organization (WHO) [1–3]. More than 12 million people, including children, receive cancer diagnoses for the first time each year, and seven million people die from the disease [4]. Cancer treatments make patients immunosuppressed which is the main reason for secondary infections by several kinds of microorganisms [5]. In this context, the dual effect coming out from drugs and agents is a promising approach to solving many problems with agents and possibly with low doses. However, these kinds of agents usually lack compatibility which releases severe side effects [6]. Biocompatible agents are a wide group of biomaterials that are characterized by unique cytocompatibility and low toxicity [7].

Among different biomaterials, biopolymers are a group of biological natural polymers produced by living organisms that are compatible with the biological system from which they originate [8,9]. In summary, the formulation of drugs or biologically active agents into biopolymers enhances activity and reduces side effects [10–13]. Cellulose and its derivatives have paved the way for biopolymers in this particular field [14–16]. Ethyl cellulose (EC) is an ether cellulose derivative used in sustained-release dosage forms as tablets or capsules. EC is frequently utilized as a polymer that controls the place of breakdown. Therefore, it is a non-toxic, stable, compressible, passive, hydrophobic polymer that has frequently been used to manufacture medicinal dosage forms due to its low cost, ease of manufacturing, and non-toxicity. For both soluble and poorly soluble pharmaceuticals, the characteristics of EC sustained-release products, including film-coated tablets, microspheres, microcapsules, and matrix tablets, have been documented. To stabilize different medications against unintended interactions, EC is employed to microencapsulate them. It has been utilized as a particle emulsion stabilizer, a polymeric covering, and controlled release in oral formulations, transdermal films, and patches [17,18]. Moreover, collagen is a biopolymer which is the primary structural protein of the extracellular matrix present in the different connective tissues of the body [19]. It makes up between 25% and 35% of the protein in a mammal's entire body and is the basic building block of connective tissue [20]. The collagen helix, a triple helix of an extended fibril made of amino acids, is what makes up collagen. It is mostly present in connective tissue, which includes skin, tendons, ligaments, cartilage, and bones [21–24].

On the other hand, metal nanoparticles (NPs) are considered potentially biologically active materials in various fields, such as the medical and pharmaceutical industries [25]. The usage of titanium oxide nanoparticles (TiO_2 NPs) among inorganic nanoparticles has been widespread, including uses in food packaging, plastics, cosmetics, and textile sectors [26]. Physicochemical techniques such as microemulsion, chemical precipitation, hydrothermal crystallization, and sol-gel procedures have all been used in the past to create TiO_2 NPs. The potential applications of physicochemical approaches in their synthesis are constrained by the need for pressure, high temperatures, and poisonous substances. As a result, less harmful methods for producing NPs on a greater scale have been developed. Given that, biological extracts are the most suitable reducing agents in the green (eco-friendly) method since they act as both a reducing agent and a stabilizing agent for the produced nanoparticles. Additionally, over the years, there has been a lot of investigation over the inherent characteristics of Cr_2O_3 nanoparticles. It has been found that trivalent is more stable than other forms of chromium oxide NPs, as is distinguished by its improved resistivity, hardness, and thermodynamic stability [27]. In general, Cr_2O_3 is a semiconductor that depends on the development circumstances due to its high refractive index. It has been utilized as a low- and medium-temperature selective solar absorber and has also been reported to reveal antibacterial and anticancer effects [28].

Moreover, the bimetallic nanoparticle is a new promising nanostructure that is used potentially in medical, pharmaceutical and many other advanced techniques [29,30]. Combining two metals in one bimetallic nanoparticle provides a greater degree of freedom to

alter the particle properties, making this an attractive area of research. Bimetallic nanoparticles and composites have garnered significant attention in recent years for their potential applications in various biological contexts. Specifically, they are being explored for their efficacy as agents in the fields of oncology and antimicrobial therapy. In anticancer applications, bimetallic nanoparticles demonstrate promise due to their unique physicochemical properties. These nanoparticles can be engineered to exhibit enhanced targeting capabilities, enabling them to selectively accumulate in cancerous tissues while minimizing damage to healthy cells. Additionally, their surface chemistry can be tailored to facilitate drug delivery, making them potential carriers for chemotherapeutic agents. Moreover, the synergistic effects of combining two different metals in a nanoparticle structure can lead to improved therapeutic outcomes, such as enhanced cytotoxicity against cancer cells. In antimicrobial applications, bimetallic nanoparticles and composites have shown potential as effective agents against a broad spectrum of microorganisms. The combination of different metals can impart a synergistic antimicrobial effect, making these nanoparticles particularly effective against drug-resistant strains of bacteria and fungi. Their high surface area and reactivity also contribute to their antimicrobial efficiency. This increases their usefulness in imaging, biology, and catalysis with noticeable synergetic effect of both components, even in biological applications as anticancer and antimicrobial agents. The controlled synthesis and functionalization of these nanoparticles allows for customization of their properties to suit specific biological applications. Surface modifications with biomolecules or polymers can enhance stability, biocompatibility, and targeted delivery. It is worth noting that while bimetallic nanoparticles and composites hold immense promise, further research is required to fully understand their behavior in complex biological environments and to address any potential toxicity concerns. Additionally, the development of scalable and cost-effective synthesis methods will be crucial for their translation into clinical applications. [31,32].

Unfortunately, the release of nanoparticles has a damaging effect that destroys cell biosystems [33]. In light of the above, the formulation of nanocomposites based on nanoparticles is an auspicious way to produce safe and controlled nanoparticles, especially when formulated in a nanocomposite that amplifies their activity.

Herein, the formulation of materials as nanocomposite could enhance bimetallic nanoparticle performance [34]. The constituent materials are combined to produce a material with characteristics that are distinct from the constituent parts, despite having chemical or physical qualities that are noticeably different [35].

Therefore, in the current work, a new promising formulation of bimetallic nanoparticles ($\text{TiO}_2@\text{Cr}_2\text{O}_3$) was synthesized *in situ* in the presence of collagen, and ethyl cellulose was used as a capping and stabilizing agent. Moreover, the biopolymers played a dual role as a capping agent as well as an induction for biocompatibility. The formulated nanocomposite was characterized using a physicochemical and topographical analysis as well, and the biological activity including antimicrobial activity, cytotoxicity and anticancer activity was evaluated.

2. Materials and Methods

2.1. Materials

Collagen (bovine Achilles tendon), ethyl cellulose (viscosity 4 cP, 5% in toluene/ethanol 80:20 (*v/v*) and 48% ethoxyl were purchased from Sigma-Aldrich, Germany. Titanium (IV) chloride and chromium (III) nitrate nonahydrate were used as precursors for nanoparticle formulation. Microbial and cell line media and reagents were purchased from Loba Chem, Maharashtra, India, in analytical grade.

2.2. Preparation of Nanocomposites

The environmentally friendly *in situ* synthesis and formulation of $\text{TiO}_2@\text{Cr}_2\text{O}_3$ NPs were conducted using collagen and ethyl cellulose. Collagen was dissolved in deionized water at a concentration of 1% (*w/v*), while ethyl cellulose was dissolved in ethanol at a concentration of 1% (*w/v*). Subsequently, the ethyl cellulose solution was added dropwise

to the collagen solution while vigorously stirring for 1 h at 70 °C. This resulted in the appearance of a milky yellowish color. The mixture was then transferred to an ultrasonic water bath and maintained at 70 °C for 2 h. Aqueous solutions of metal salts, specifically 10 mL of 1% (*w/v*) titanium (IV) chloride and 5 mL of 1% (*w/v*) chromium (III) nitrate nonahydrate, were added during this process. The resulting solution was mixed under continuous stirring for 1 h and subsequently sonicated using an ultrasonic probe for 15 min. The prepared nanocomposite was washed with 70% ethanol three times, followed by lyophilization. The final product was stored in a refrigerator for future use.

2.3. Characterization

The synthesized nanocomposites were characterized through physicochemical and morphological investigations, with comparisons made to its individual constituents. Physicochemical analysis included ultraviolet-visible (UV-VIS) spectroscopy (Jasco, V-630, Tokyo, Japan) within the 200–1000 nm range. Fourier-transform infrared (FTIR) measurements were conducted using an Impact-400 FT-IR spectrometer (Nicolet Analytical Instruments, 5225-1, Madison, WI, USA) over the range of 400–4000 cm^{-1} . X-ray diffraction (XRD) analysis was performed at a 2θ (Bragg angle) of 5–80°, employing a Bruker D8 Advance X-ray diffractometer (Mannheim, Germany). Furthermore, a high-resolution transmission electron microscope (HRTEM) JEOL 2010, Tokyo, (Japan) operating at 300 kV was utilized for the morphological study, enabling examination of particle shape and size, along with selected area electron diffraction (SAED) patterns. The field emission scanning electron microscopy (SEM) coupled with Energy Dispersive X-ray Analysis (EDX), Model Quanta 250 FEG (Field Emission Gun), facilitated additional morphological analysis. Thermal stability assessment was carried out using an SDT Q600 thermal analyzer from TA Instruments-Waters LLC (Billerica, MA, USA) in a nitrogen atmosphere, with a heating rate of 10 °C/min.

2.4. Biological Profile

Cytotoxicity tests, antibacterial activity, and antioxidant activity were included in the biological profile examination. The MTT procedure [36] was used to assess the cytocompatibility of the nanocomposite against the normal cell lines, namely WI38 (normal fibroblasts derived from lung tissue) and the normal Vero fibroblast cells as well as the cancer cell lines, including MCF7 (breast carcinoma) (marked in women) and A549 (lung carcinoma) (marked in men) cell lines that were obtained from the American Type Culture Collection (ATCC). The number of cells and the percentage of viable cells were determined using Equation (1):

$$\text{Viability \%} = \frac{\text{Test OD}}{\text{Control OD}} \times 100 \quad (1)$$

where the Test OD is the obtained absorbance of the sample and the Control OD is the obtained absorbance of the control.

IC_{50} value was calculated according to our previous study [12]. Additionally, the turbidimetric test was used in our earlier study [37] with an initial nanocomposite concentration of 100 $\mu\text{g}/\text{mL}$ to assess the antibacterial activity. The minimal inhibition concentration (MIC) was evaluated. Gram-positive (*Staphylococcus aureus* ATCC 25923, *Bacillus subtilis* ATCC 6051), Gram-negative (*Pseudomonas aeruginosa* ATCC 27853, *Escherichia coli* ATCC25922), unicellular fungi (*Candida albicans* ATCC90028), and filamentous fungi (*Aspergillus niger* RCMB 02724) were used in this study against formulated nanocomposite. It was reported that the killing assay would take 24 h for bacteria and unicellular fungi, and 72 h for filamentous fungi with some minor adjustments [38].

According to previous studies, the antioxidant activity assessment was performed using the radical scavenging ability of the 2,2-diphenyl-1-picrylhydrazyl (DPPH) method [39]. The tested samples were produced at various concentrations via serial dilution of nanocomposite 100–0 $\mu\text{g}/\text{mL}$ to evaluate the formulated nanocomposite antioxidant behavior.

2.5. Statistical Analysis

All findings were calculated using the mean value of three replicates and standard errors. Results were subjected to analysis-of-variance means using the Minitab 17 program.

3. Results and Discussion

The formulation of bimetallic nanoparticles was carried out via a green method to enhance their activity and reduce the side effects due to the use of collagen and ethyl cellulose. The biopolymers were not used only in the formulation of bimetallic nanoparticles but also were acting as a capping and stabilizing agent for bimetallic nanoparticle synthesis. The formulated nanocomposite was characterized via physicochemical, topographic and biological processes.

3.1. Characterization

The bimetallic nanoparticles as well as the formulation of these particles into the nanocomposite were investigated using UV-VIS spectrophotometry and TEM. UV-VIS analysis is a common technique used to study the electronic transitions and optical properties of materials. The absorption bands in a UV-VIS spectrum correspond to the energy levels at which electrons in the material absorb photons, leading to electronic transitions. The existence of characteristic absorbance peaks was verified through the synthesis of nanoparticles and their subsequent encapsulation within a biopolymer structure. TEM is a powerful imaging technique that allows for high-resolution visualization of materials at the nanoscale. The UV-VIS spectrum of nanocomposite (Figure 1) showed four peaks: a small one at 300 nm and a broad peak at 353 nm which confirmed the formulation of TiO_2 NPs [40–42]. Additionally, a small peak at 393 and a high peak at 421 nm were observed which refer to Cr_2O_3 NPs [43]. The marked difference in positions of nanoparticles could be assigned to the trapping of nanoparticles into nanocomposite structure as well as the attraction between nanoparticles to each other. When two different metal elements are present in the nanoparticles, their electronic properties can interact, leading to shifts or splitting of absorption bands. This phenomenon can result in the appearance of multiple absorption peaks. The combination of different metal elements can create new energy levels that affect the electronic transitions, and this interaction can alter the position of the absorption bands compared to the individual metals. Also, when biopolymers are involved in the synthesis or stabilization of nanoparticles, they can form a network around the nanoparticles, creating a matrix that influences their electronic and optical properties. This can result in changes to the energy levels at which absorption occurs, potentially leading to the appearance of additional absorption bands or shifts in the existing bands. The interaction between the nanoparticles and the biopolymers can modify the nanoparticles' surface chemistry and affect their plasmonic behavior [39].

High-resolution TEM images with different magnifications are presented in Figure 2. The low magnification image in Figure 2a illustrates a nanostructure network decorated with spots that arise from metal oxide nanoparticles. At a higher magnification (Figure 2b), the bimetallic nanoparticles become more evident. These nanoparticles have irregular shapes that suggest variability in size. A closer look (Figure 2c) reveals a network made up of nanospheres and nanorods. This network appears to be composed of spheres that are interconnected by nanorods. The surface texture of this network is rough, indicating a complex three-dimensional arrangement. Moreover, the high-magnification TEM image (Figure 2c) implies that the particles of bimetallic were distributed over the surface as a small sphere that is referred to as TiO_2 NPs, and rods are referred to as Cr_2O_3 NPs. In addition, the SEAD pattern of nanocomposite (Figure 2d) shows a typical polycrystalline behavior with circles arranged together without spots. Based on the TEM study, it is concluded that the nanocomposite was formulated as a nanostructure network that traps the bimetallic nanoparticles inside.

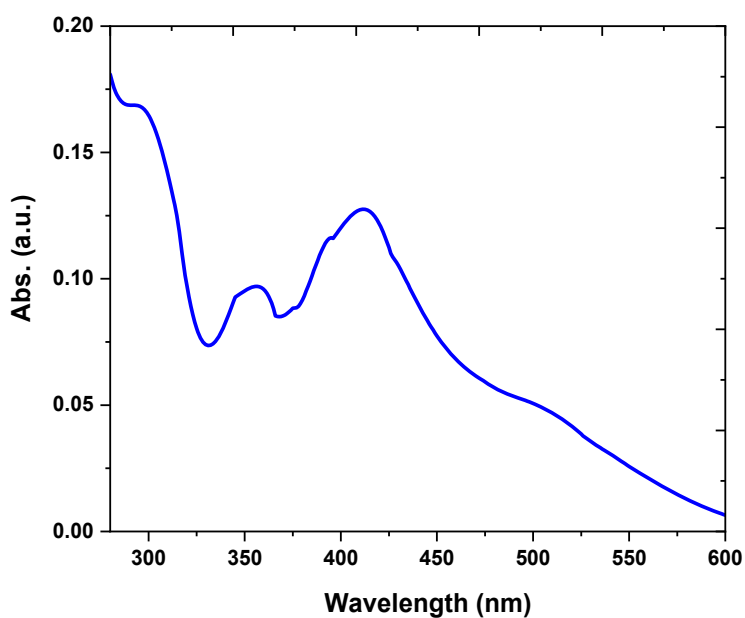


Figure 1. UV-VIS spectrum of formulated nanocomposite.

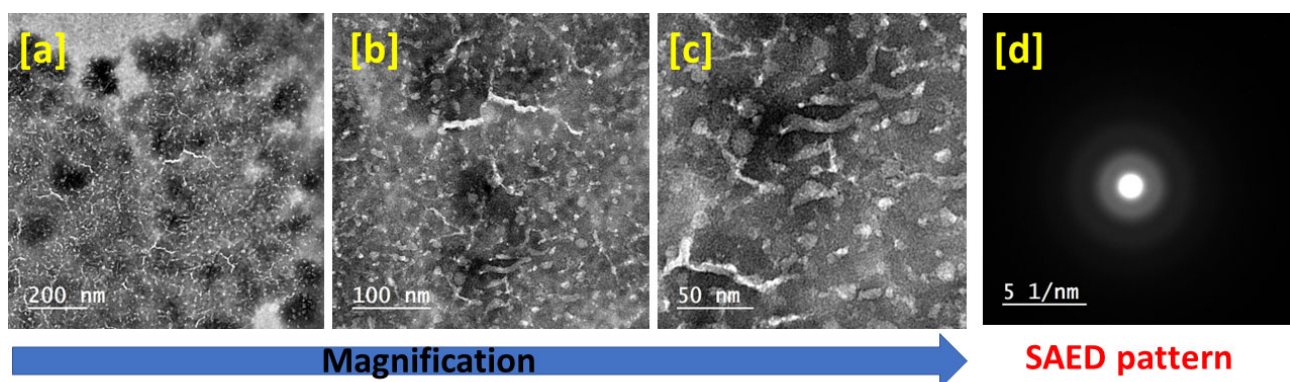


Figure 2. High-resolution TEM images with different magnifications (low, moderate and high at (a–c), respectively) as well as the SAED pattern (d).

The molecular structure of the formulated nanocomposite compared with the parent materials was studied via FTIR as presented in Figure 3. FTIR analysis revealed the functional groups and their changes during nanocomposite formulation. The neat ethyl cellulose spectrum revealed a strong band at 3436 cm^{-1} that is attributed to the stretching mode of hydroxyl groups [44]. Another band was observed at range $2971\text{--}2870\text{ cm}^{-1}$ which was assigned to CH_3 and CH_2 asymmetric and symmetric stretching modes of methyl and ethyl groups. The band at 1731 cm^{-1} and a small one at 1636 cm^{-1} corresponded to C=O starching vibration [45]. Moreover, the main sharp band at 1052 cm^{-1} arises from the carbohydrate linkage. The neat collagen presented the main functional group bands at 3279 , 3063 cm^{-1} which correspond to OH and NH groups overlapping stretching vibrations [46]. The bands at 2926 , 1627 , 1523 and 1226 cm^{-1} represented the main amide forms: amid B, amid I, amid BII and amid III, repetitively [47]. On the other hand, the nanocomposite spectrum showed significant changes in the main functional groups. The OH group peak shows a new position compared with parent materials (3279 cm^{-1}) with a broadness. In addition, the CH group region revealed obvious changes in the bands' position and intensity. Moreover, the C=O band disappeared or noticed as a small band. In this context, the functional groups of the nanocomposite bands were presented with changes in the position and intensity as well as behavior and appearance in comparison to their neat material bands, that emphasized the interaction between biopolymers and also could be a result of

the presence of bimetallic nanoparticles. Furthermore, the carbohydrate linkage band in ethyl cellulose and amide bands in collagen were presented in the nanocomposite spectrum affirming the structure of both biopolymers, whereas the inorganic nanoparticles bands were noticed in the fingerprint region where the TiO_2 NPs band was located at 679 cm^{-1} assigned to O-Ti-O stretching [48–50]. However, the presence of Cr_2O_3 NPs was indicated according to bands at 869 and 511 cm^{-1} referring to Cr=O and Cr-O bonding [51,52]. In summary, the Fourier-Transform Infrared (FTIR) study likely provided insights into the chemical interactions and bonding within the nanocomposite formulation and bimetallic synthesis. This analysis is essential for understanding the molecular structure, functional groups, and potential reactions that take place during the preparation of the nanocomposite. The favorable outcomes observed in UV-VIS and TEM analyses further strengthen the credibility of these conclusions.

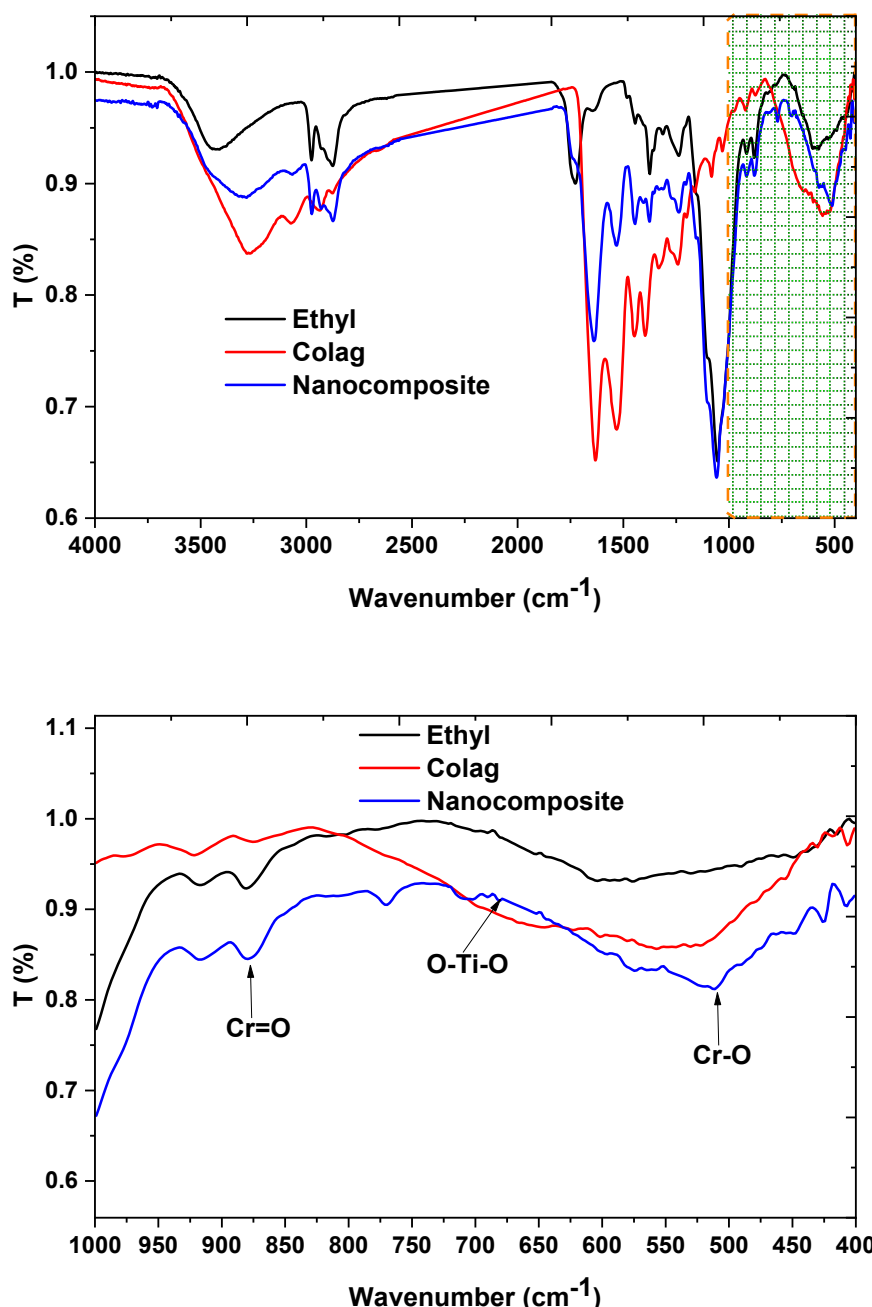


Figure 3. FTIR spectra of formulated nanocomposite and its parent materials. Ethyl stands for ethyl cellulose; Colag stands for collagen.

XRD crystallography patterns were shown in Figure 4 for nanocomposite and neat ethyl cellulose and collagen. It is well known that the pure biopolymer crystallography pattern did not contain many peaks due to lack of crystallinity. Pure ethyl cellulose was observed with a strong hump peak at around $2\theta = 20^\circ$ which is typically found in the ethyl cellulose pattern [53]. However, the collagen pattern showed further details compared with ethyl cellulose showed a small peak at $2\theta = 6.5^\circ$ and a less sharp peak at $2\theta = 20^\circ$ as well as a broad peak at $2\theta = 30^\circ$ and those peaks were recorded in previous literature [54,55]. Likewise, the nanocomposite pattern showed more crystalline behavior in comparison with the neat materials and observed a new peak at $2\theta = 15.2^\circ$ that could be a result of the interaction of the biopolymer networks and the doping effect of bimetallic nanoparticles. Additionally, the main peak of the biopolymer decreased in intensity. Also, the bimetallic nanoparticles were presented where TiO_2 NPs peaks were assigned at $2\theta = 30.9, 32, 36, 45^\circ$ [56–58] and Cr_2O_3 NPs at $2\theta = 33, 36, 50, 64^\circ$ [59–61] as small peaks according to the presence of biopolymers and trapping of bimetallic into biopolymer chains. These observations were in good agreement with other physiochemical and TEM analyses.

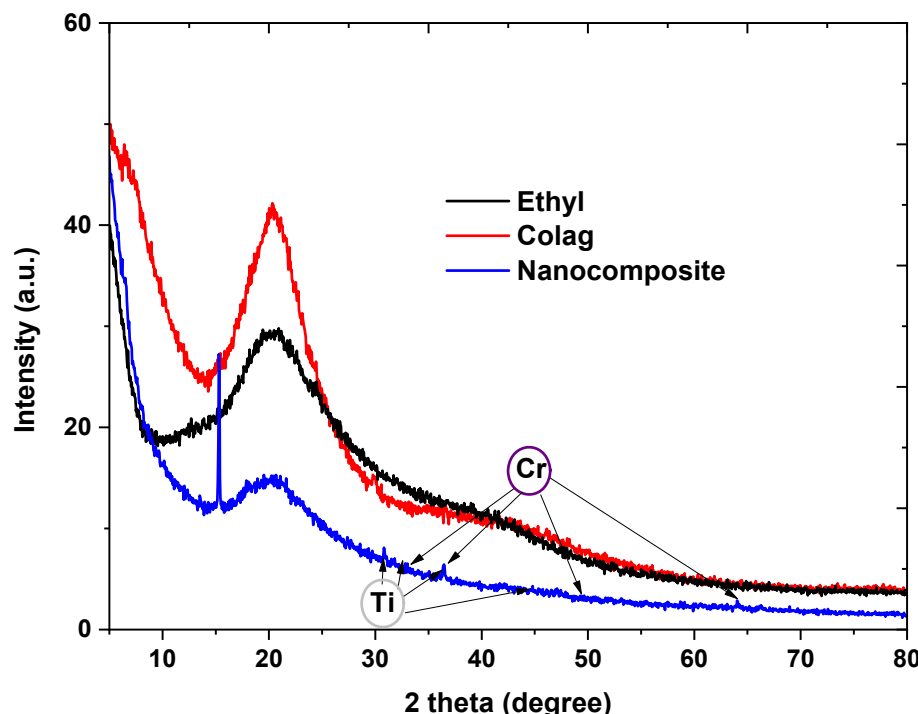


Figure 4. XRD crystallography pattern of formulated nanocomposite and its parent materials. Ethyl stands for ethyl cellulose; Colag stands for collagen.

SEM study for biopolymers and nanocomposite as well as EDX and mapping for nanocomposite are presented in Figure 5. The neat ethyl cellulose SEM image (Figure 5a) presented as a typical cellulose derivative with many cracks and a smooth surface texture [62]. The neat collagen SEM image (Figure 5b) showed irregular surface behavior with some pores that could be attributed to the helix interaction [63]. The nanocomposite SEM images with low magnification (Figure 5c) presented a new surface behavior in comparison with neat materials with shiny dots on the surface and were uniformly distributed. Moreover, the high-magnification SEM image of the nanocomposite (Figure 5d) showed the surface texture's spongy-like appearance that is a nice match with the nanocomposite-based biopolymers' morphology [64]. Furthermore, the EDX chart of the nanocomposite showed the presence of carbon and oxygen atoms originating from formulated ethyl cellulose, collagen and bimetallic nanoparticles. The presence of nitrogen ions arises from collagen with carbon and oxygen as well. In the mapping, the Ti and Cr atoms emphasized the homogenous distribution of bimetallic particles.

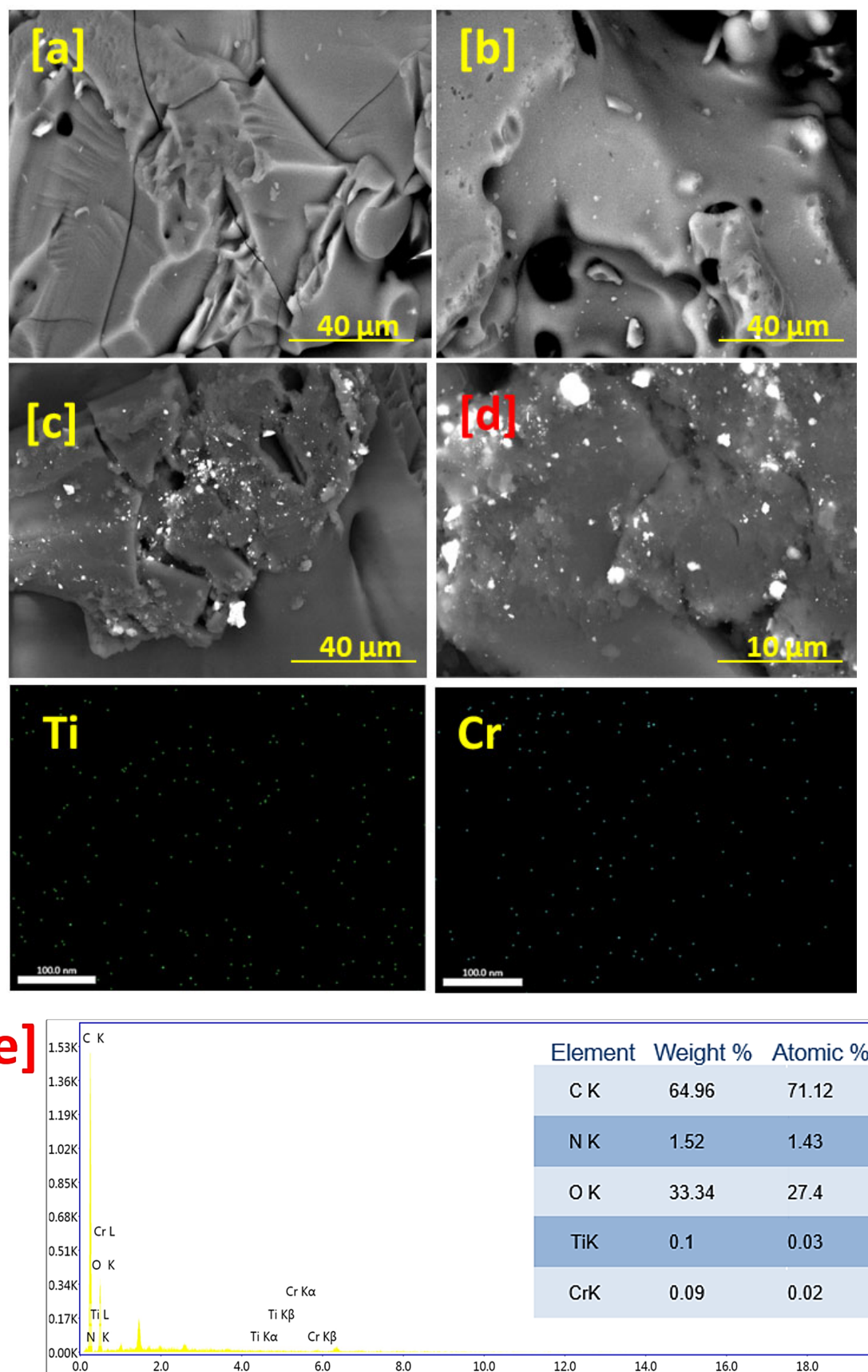


Figure 5. SEM images of ethyl cellulose (**a**), collagen (**b**) and nanocomposite with low magnification (**c**), and high magnification (**d**), and EDX mapping of nanocomposite (**e**).

3.2. Biological Profile

Biological activities were tested for the formulated nanocomposite including cytotoxicity evaluation against normal cell lines as well as anticancer activity against cancer cell lines, as one of them is related to major cancer in women (breast carcinoma) and another presented the common cancer in men (lung carcinoma). In addition, the antimicrobial test was carried out against common infectious microorganisms including bacteria and fungi. The antioxidant activity was carried out using a DPPH test.

3.3. Cytotoxicity Assays

In vitro evaluation of cytotoxicity and anticancer activity are presented in Figure 6. The cytotoxicity of the formulated nanocomposite (Figure 6a) showed a good agreement with high IC₅₀ for Vero and WI38, which were found at concentrations of 40.4 and 52 µg/mL, respectively. On the other hand, the anticancer activity IC₅₀ of nanocomposite was recorded at 19 and 22 µg/mL for MCF7 and A549, respectively. Worthwhile, the statistical analysis presented in Figure 6b indicates that the anticancer activity of formulated nanocomposite was recorded for both types of cancer cell lines as a significant effect at low concentrations. The above findings revealed that the nanocomposite showed a kind of selectivity to cancer cells. Furthermore, the IC₅₀ values against normal cells were recorded higher than ones of cancer cells, which means the nanocomposite affects the cancer cells more than normal cells. These observations imply the importance of nanoparticle formulation that enhanced the material's biological selectivity. Accordingly, the photoactivity of TiO₂NPs played a crucial role in anticancer activity that has been enhanced with Cr₂O₃NPs, destroying the cancer cells organelles, especially the cytoplasmic fluid [65,66]. Nevertheless, here an important question arises: why does the nanocomposite severely affect the cancer cells and mildly affect the normal cells? As the most key feature, the nanocomposite was based on biocompatible biopolymers where the collagen is a component of many cells and ethyl cellulose is mildly interacting with the biological cells. Moreover, the nanocomposite structure facilitated the enhanced bimetallic nanoparticles' effect with control of the nanoparticles' release as well.

3.4. Antimicrobial Activity

Figure 7 shows the antimicrobial activity of formulated nanocomposite including MIC and time required for killing. The MIC values of tested microorganisms (Figure 7a) were recorded as 3.12, 3.12, 12.5, 6.25, 12.5 and 50 µg/mL for *S. aureus*, *B. subtilis*, *P. aeruginosa*, *E. coli*, *C. albicans* and *A. niger*, respectively. Obviously, the antimicrobial activity was achieved as a nice broad spectrum and antifungal active nanocomposite with low MIC values for all tested microbial populations, whereas the antimicrobial activity was gained from the synergistic effect between TiO₂NPs and Cr₂O₃NPs. The TiO₂NPs mechanism of action improved with superoxide anion radicals, which act as a strong oxidizing agent. Moreover, TiO₂NPs have photocatalytic reactivity that enhances the microorganism's cell killing effect [67]. The Cr₂O₃NPs played a strong role in disrupting the microbial cell organelles including cell membrane, cytoplasmic fluid and nucleic acid leading to cell prefiliation destruction [68]. Moreover, the bimetallic nanoparticles induced the reactive oxygen species (ROS) and killed the microorganism [65]. The above results confirmed that many modes of action were synergistic to enhance the antimicrobial activity as well as the time required for killing, and all observations are presented in Figure 7b. The short time required to kill all bacterial stains and unicellular fungi was recorded as 12 h and for filamentous fungi was recorded as 42 h. The time needed to kill all presented Gram-positive bacteria was about 10 h and for Gram-negative bacteria was about 12 h. On the other side, the time needed to kill unicellular fungi was recorded as 12 h and for filamentous fungi was extended to 42 h according to the slow rate of higher filamentous fungi in comparison with the other kinds of microbes. In this manner, the nanocomposite presented a great antimicrobial activity against most microbial pathogens with a fast rate of killing as well.

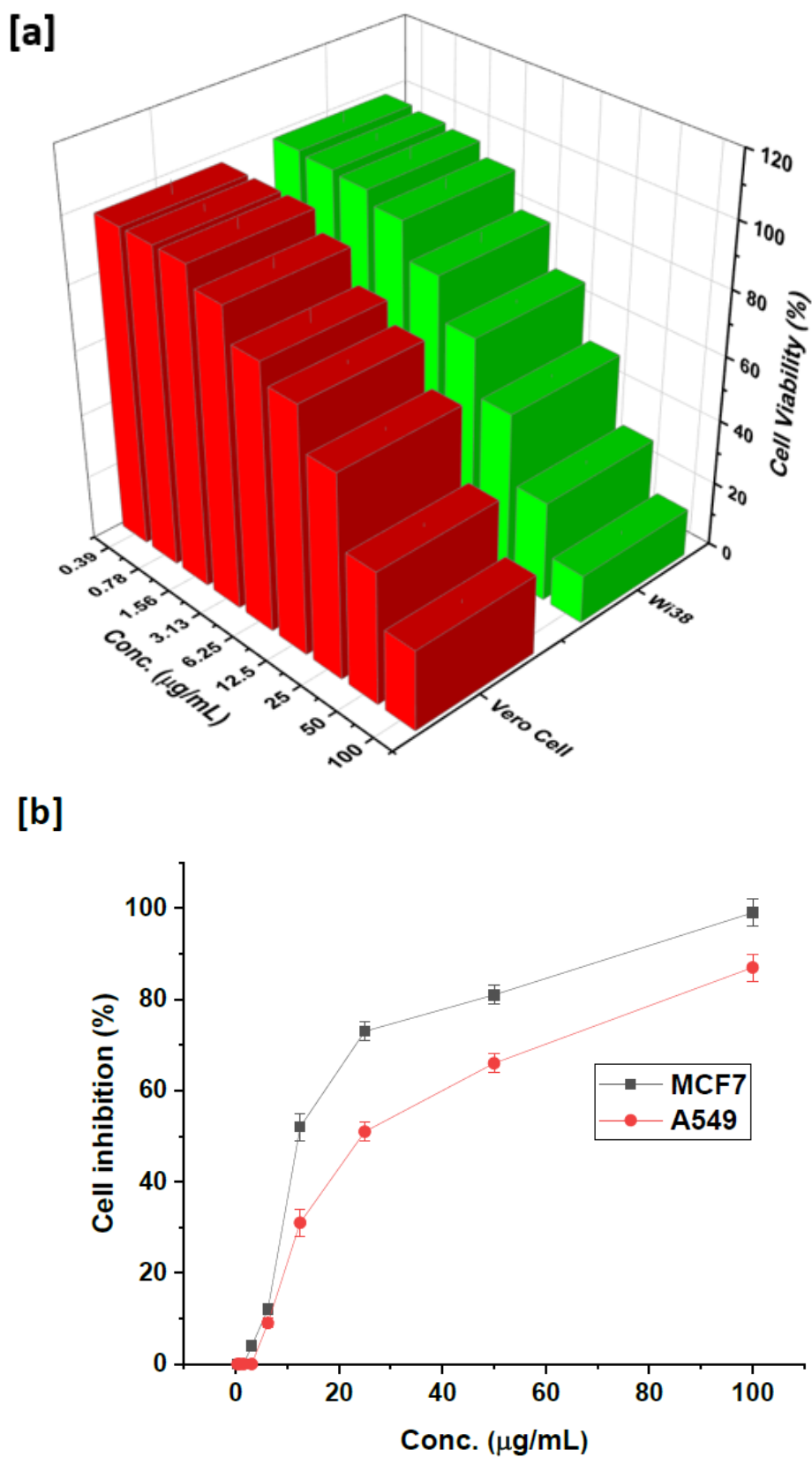


Figure 6. Cytotoxicity assay (a) and anticancer activity assay (b) for formulated nanocomposite.

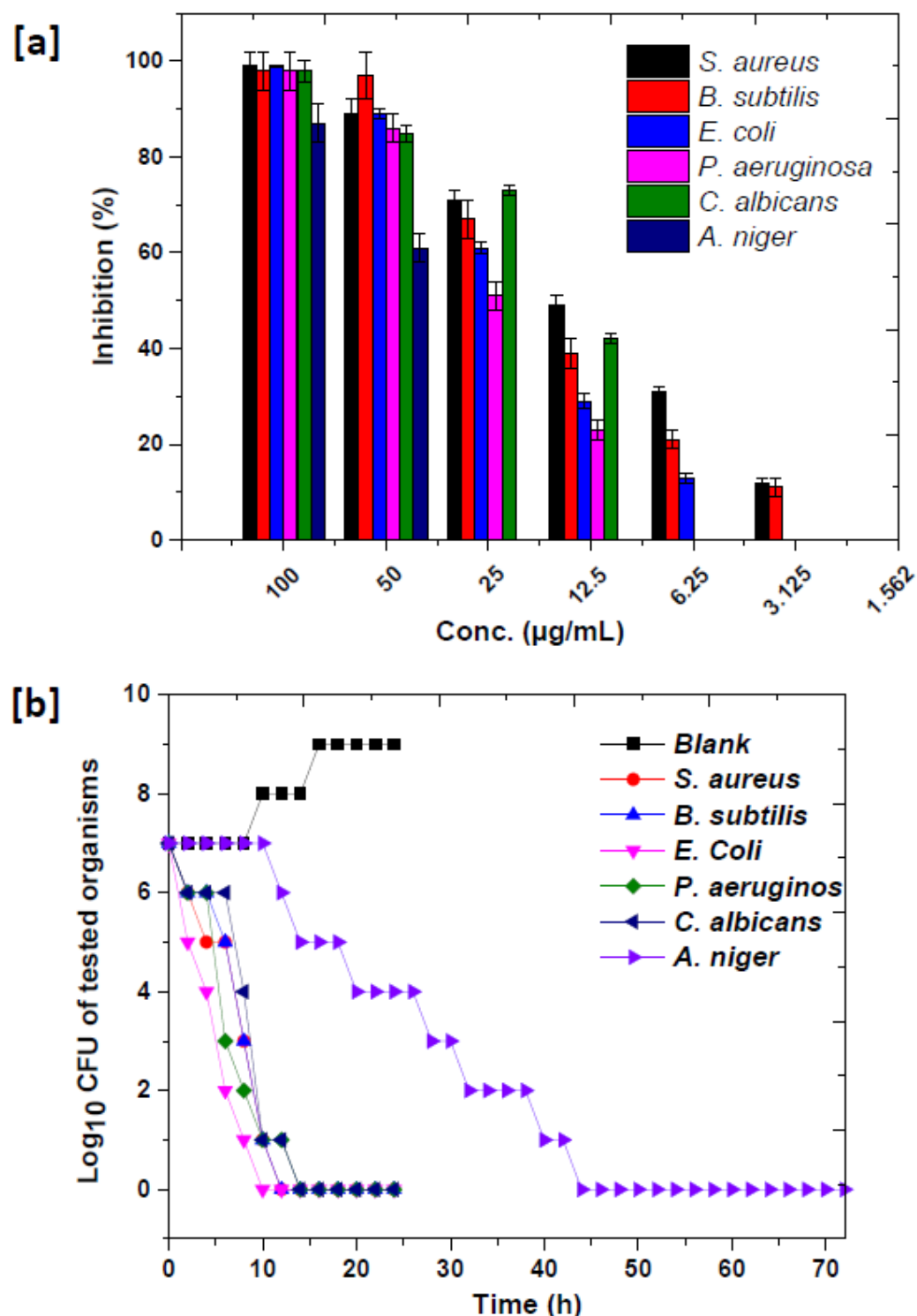


Figure 7. Antimicrobial study of formulated nanocomposite: (a) MIC calculations and (b) the time required for killing.

3.5. Antioxidant Activity

The antioxidant activity of the formulated nanocomposite is illustrated in Figure 8 with statistical calculations. Serial dilution of nanocomposite 100–0 $\mu\text{g}/\text{mL}$ was tested to assign the antioxidant activity of nanocomposite. Pure ethyl cellulose did not show a nice antioxidant activity [69] compared with collagen [70], TiO_2NP [71] and $\text{Cr}_2\text{O}_3\text{NPs}$ [72]. As a result, the nanocomposite structure and components revealed an antioxidant activity where

all antioxidant capabilities enhance the efficiency of hydrogen suppliers or free-radical scavengers (FRS) of DPPH [73]. These findings validated the efficiency of the extraction procedure, which conserved the unique properties of the produced nanocomposite in addition to highlighting the antioxidant qualities of the nanocomposite with assigned antioxidant activity at 1.5 $\mu\text{g}/\text{mL}$. In summary, these findings confirm that the formulated nanocomposites worked as a strong antioxidant agent as a result of both the nanostructure and the neat materials and their composition as well.

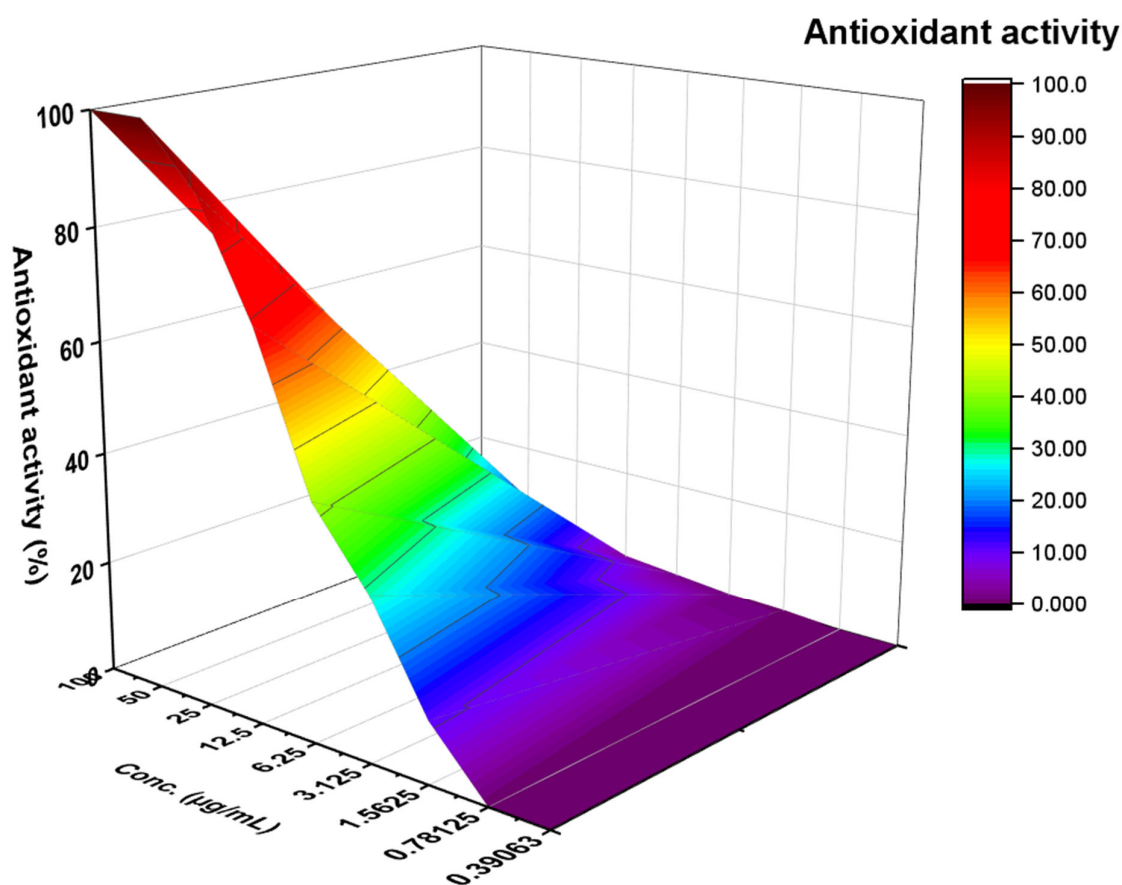


Figure 8. Antioxidant activity of formulated nanocomposite.

4. Conclusions

In conclusion, the developed nanocomposite was synthesized using ethyl cellulose and collagen as precursors for the *in situ* synthesis of bimetallic nanoparticles, specifically $\text{TiO}_2@\text{Cr}_2\text{O}_3$ nanoparticles. Through comprehensive physicochemical analyses, it was evident that the nanocomposite exhibited nanoscale characteristics, and the incorporated bimetallic nanoparticles were effectively incorporated within the nanostructure of the matrix. Surface morphology further confirmed the nanoscale dimensions of both the nanocomposite and the bimetallic nanoparticles. Biological assessments demonstrated a synergistic effect between its components. This synergy rendered the nanocomposite biocompatibility with normal cell lines and displayed notable anticancer properties, underscored by its selective targeting ability. The nanocomposite also exhibited a potent and broad-spectrum antimicrobial capability, effectively acting against various microorganisms including fungi. Additionally, the nanocomposite displayed significant antioxidant activity at a low concentration of 1.5 $\mu\text{g}/\text{mL}$. Collectively, the synthesized nanocomposite emerged as a multifunctional biological agent with diverse beneficial properties. Its nano-sized structure, effective bimetallic nanoparticle incorporation, biocompatibility with normal cells, anticancer activity, antimicrobial and antifungal capabilities, and potent antioxidant activity

collectively highlight its potential for applications in various fields such as biomedicine, materials science, and pharmaceuticals. The formulated nanocomposite represents a significant advancement in the realm of multifunctional biological agents with promising implications for numerous applications. Further research could explore its potential in specific medical treatments, materials engineering, and other relevant areas.

Author Contributions: Conceptualization, M.S.H., Y.E., S.M.S.A.-H., Y.F., T.M., O.A.A.-Q., M.E.F. and M.B.; methodology, M.S.H., Y.E., S.M.S.A.-H., Y.F., T.M., O.A.A.-Q., M.E.F. and M.B.; software, M.S.H., Y.E., S.M.S.A.-H., Y.F., T.M., O.A.A.-Q., M.E.F. and M.B.; validation, M.S.H., Y.E., S.M.S.A.-H., Y.F., T.M., O.A.A.-Q., M.E.F. and M.B.; formal analysis, M.S.H., Y.E., S.M.S.A.-H., Y.F., T.M., O.A.A.-Q., M.E.F. and M.B.; investigation, M.S.H., Y.E., S.M.S.A.-H., Y.F., T.M., O.A.A.-Q., M.E.F. and M.B.; resources, M.S.H., Y.E., S.M.S.A.-H., Y.F., T.M., O.A.A.-Q., M.E.F. and M.B.; data curation, M.S.H., Y.E., S.M.S.A.-H., Y.F., T.M., O.A.A.-Q., M.E.F. and M.B.; writing—original draft preparation, M.S.H., Y.E., S.M.S.A.-H., Y.F., T.M., O.A.A.-Q., M.E.F. and M.B.; writing—review and editing, M.S.H., Y.E., S.M.S.A.-H., Y.F., T.M., O.A.A.-Q., M.E.F. and M.B.; visualization, M.S.H., Y.E., S.M.S.A.-H., Y.F., T.M., O.A.A.-Q., M.E.F. and M.B. All authors have read and agreed to the published version of the manuscript.

Funding: This research was funded by the Deputyship for Research and Innovation, “Ministry of Education” in Saudi Arabia (IFKSUOR3-273-3).

Data Availability Statement: The datasets generated during and/or analyzed during the current study are available from the corresponding author on reasonable request.

Acknowledgments: The authors extend their appreciation to the Deputyship for Research & Innovation, Ministry of Education in Saudi Arabia, for funding this research work through project no. (IFKSUOR3-273-3).

Conflicts of Interest: The authors declare no conflict of interest.

References

1. Singh, D.; Vignat, J.; Lorenzoni, V.; Eslahi, M.; Ginsburg, O.; Lauby-Secretan, B.; Arbyn, M.; Basu, P.; Bray, F.; Vaccarella, S. Global estimates of incidence and mortality of cervical cancer in 2020: A baseline analysis of the WHO Global Cervical Cancer Elimination Initiative. *Lancet Glob. Health* **2023**, *11*, e197–e206. [[CrossRef](#)] [[PubMed](#)]
2. Karacin, C.; Oksuzoglu, B.; Demirci, A.; Keskinkılıç, M.; Baytemür, N.K.; Yılmaz, F.; Selvi, O.; Erdem, D.; Avşar, E.; Paksoy, N. Efficacy of subsequent treatments in patients with hormone-positive advanced breast cancer who had disease progression under CDK 4/6 inhibitor therapy. *BMC Cancer* **2023**, *23*, 136. [[CrossRef](#)]
3. Snaman, J.M.; Mazzola, E.; Helton, G.; Feifer, D.; Morris, S.E.; Clark, L.; Baker, J.N.; Wolfe, J. Early Bereavement Psychosocial Outcomes in Parents of Children Who Died of Cancer with a Focus on Social Functioning. *JCO Oncol. Pract.* **2023**, *19*, e527–e541. [[CrossRef](#)] [[PubMed](#)]
4. Kucerova, P.; Cervinkova, M. Spontaneous regression of tumour and the role of microbial infection—Possibilities for cancer treatment. *Anticancer Drugs* **2016**, *27*, 269–277. [[CrossRef](#)]
5. Wang, T.; Zhang, J.; Wang, Y.; Li, Y.; Wang, L.; Yu, Y.; Yao, Y. Influenza-trained mucosal-resident alveolar macrophages confer long-term antitumor immunity in the lungs. *Nat. Immunol.* **2023**, *24*, 423–438. [[CrossRef](#)] [[PubMed](#)]
6. Xiang, Y.; Guo, Z.; Zhu, P.; Chen, J.; Huang, Y. Traditional Chinese medicine as a cancer treatment: Modern perspectives of ancient but advanced science. *Cancer Med.* **2019**, *8*, 1958–1975. [[CrossRef](#)]
7. Hasanin, M.S. Cellulose-based biomaterials: Chemistry and biomedical applications. *Starch Stärke* **2022**, *74*, 2200060. [[CrossRef](#)]
8. Abdelraof, M.; Ibrahim, S.; Selim, M.; Hasanin, M. Immobilization of L-methionine γ -lyase on different cellulosic materials and its potential application in green-selective synthesis of volatile sulfur compounds. *J. Environ. Chem. Eng.* **2020**, *8*, 103870. [[CrossRef](#)]
9. Hasanin, M.S. Simple, economic, ecofriendly method to extract starch nanoparticles from potato peel waste for biological applications. *Starch Stärke* **2021**, *73*, 2100055. [[CrossRef](#)]
10. Hasanin, M.; Swielam, E.M.; Atwa, N.A.; Agwa, M.M. Novel design of bandages using cotton pads, doped with chitosan, glycogen and ZnO nanoparticles, having enhanced antimicrobial and wounds healing effects. *Int. J. Biol. Macromol.* **2022**, *197*, 121–130. [[CrossRef](#)]
11. Shehabeldine, A.; El-Hamshary, H.; Hasanin, M.; El-Faham, A.; Al-Sahly, M. Enhancing the antifungal activity of griseofulvin by incorporation a green biopolymer-based nanocomposite. *Polymers* **2021**, *13*, 542. [[CrossRef](#)] [[PubMed](#)]
12. Hasanin, M.; Taha, N.F.; Abdou, A.R.; Emara, L.H. Green decoration of graphene oxide Nano sheets with gelatin and gum Arabic for targeted delivery of doxorubicin. *Biotechnol. Rep.* **2022**, *34*, e00722. [[CrossRef](#)]

13. Hasanin, M.S.; Abdelraof, M.; Fikry, M.; Shaker, Y.M.; Sweed, A.M.; Senge, M.O. Development of Antimicrobial Laser-Induced Photodynamic Therapy Based on Ethylcellulose/Chitosan Nanocomposite with 5, 10, 15, 20-Tetrakis (m-Hydroxyphenyl) porphyrin. *Molecules* **2021**, *26*, 3551. [[CrossRef](#)]
14. Dürig, T.; Karan, K. Chapter 9—Binders in Wet Granulation. In *Handbook of Pharmaceutical Wet Granulation*; Narang, A.S., Badawy, S.I.F., Eds.; Academic Press: Cambridge, MA, USA, 2019; pp. 317–349.
15. Gunduz, O.; Ahmad, Z.; Stride, E.; Edirisinghe, M. Continuous Generation of Ethyl Cellulose Drug Delivery Nanocarriers from Microbubbles. *Pharm. Res.* **2013**, *30*, 225–237. [[CrossRef](#)] [[PubMed](#)]
16. Bassyouni, M.; Zoromba, M.S.; Abdel-Aziz, M.H.; Mosly, I. Extraction of Nanocellulose for Eco-Friendly Biocomposite Adsorbent for Wastewater Treatment. *Polymers* **2022**, *14*, 1852. [[CrossRef](#)]
17. Muhammin, M.; Chaerunisaa, A.Y.; Bodmeier, R. Preparation and evaluation of various formulation effects of the second emulsion on the shape and release profile of propranolol HCl from ethyl cellulose microparticle blends. *Polym. Int.* **2023**, *72*, 383–391. [[CrossRef](#)]
18. Mu, J.; Du, Y.; Li, X.; Yan, R.; Zhong, H.; Cai, M.; Yu, N.; Zhang, J.; Yuan, X.; Hua, X.; et al. Collagen-anchored cascade nanoreactors with prolonged intratumoral retention for combined cancer starvation and chemotherapy. *Chem. Eng. J.* **2023**, *451*, 138554. [[CrossRef](#)]
19. Ling, Q.; Fan, X.; Ling, M.; Liu, J.; Zhao, L.; Gu, H. Collagen-Based Organohydrogel Strain Sensor with Self-Healing and Adhesive Properties for Detecting Human Motion. *ACS Appl. Mater. Interfaces* **2023**, *15*, 12350–12362. [[CrossRef](#)]
20. Fazli, S.; Zohaib, H.; Isfahan, T.; Adeeb, S.; Fazli, W. A review on recent advances and applications of fish collagen. *Crit. Rev. Food Sci. Nutr.* **2021**, *61*, 1027–1037. [[CrossRef](#)]
21. Feng, Y.; Shi, Y.; Tian, Y.; Yang, Y.; Wang, J.; Guo, H.; Banitaba, S.N.; Khademlqorani, S.; Li, J. The Collagen-Based Scaffolds for Bone Regeneration: A Journey through Electrospun Composites Integrated with Organic and Inorganic Additives. *Processes* **2023**, *11*, 2105. [[CrossRef](#)]
22. Wong, F.S.Y.; Tsang, K.K.; Chan, B.P.; Lo, A.C.Y. Both non-coated and polyelectrolytically-coated intraocular collagen-alginate composite gels enhanced photoreceptor survival in retinal degeneration. *Biomaterials* **2023**, *293*, 121948. [[CrossRef](#)] [[PubMed](#)]
23. Yuan, H.; Liu, B.; Liu, F.; Li, C.; Han, L.; Huang, X.; Xue, J.; Qu, W.; Xu, J.; Liu, W.; et al. Enhanced Anti-Rheumatoid Arthritis Activity of Total Alkaloids from Picrasma Quassiodes in Collagen-Induced Arthritis Rats by a Targeted Drug Delivery System. *J. Pharm. Sci.* **2023**, *112*, 2483–2493. [[CrossRef](#)] [[PubMed](#)]
24. Lara-Rico, R.; López-Badillo, C.M.; Claudio-Rizo, J.A.; Cabrera-Munguía, D.A.; Becerra-Rodríguez, J.J.; Espinosa-Neira, R.; Cruz-Ortiz, B.R. Smart hydrogels based on semi-interpenetrating polymeric networks of collagen-polyurethane-alginate for soft/hard tissue healing, drug delivery devices, and anticancer therapies. *Biopolymers* **2023**, *114*, e23538. [[CrossRef](#)]
25. Chandrakala, V.; Aruna, V.; Angajala, G. Review on metal nanoparticles as nanocarriers: Current challenges and perspectives in drug delivery systems. *Emergent Mater.* **2022**, *5*, 1593–1615. [[CrossRef](#)] [[PubMed](#)]
26. Hamed, M.T.; Bakr, B.A.; Shahin, Y.H.; Elwakil, B.H.; Abu-Serie, M.M.; Aljohani, F.S.; Bekhit, A.A. Novel Synthesis of Titanium Oxide Nanoparticles: Biological Activity and Acute Toxicity Study. *Bioinorg. Chem. Appl.* **2021**, *2021*, 8171786. [[CrossRef](#)] [[PubMed](#)]
27. Hassan, D.; Khalil, A.T.; Solangi, A.R.; El-Mallul, A.; Shinwari, Z.K.; Maaza, M. Physiochemical properties and novel biological applications of Callistemon viminalis-mediated α -Cr₂O₃ nanoparticles. *Appl. Organomet. Chem.* **2019**, *33*, e5041. [[CrossRef](#)]
28. Ghotekar, S.; Pansambal, S.; Bilal, M.; Pingale, S.S.; Oza, R. Environmentally friendly synthesis of Cr₂O₃ nanoparticles: Characterization, applications and future perspective—A review. *Case Stud. Chem. Environ. Eng.* **2021**, *3*, 100089. [[CrossRef](#)]
29. Roopan, S.M.; Surendra, T.V.; Elango, G.; Kumar, S.H.S. Biosynthetic trends and future aspects of bimetallic nanoparticles and its medicinal applications. *Appl. Microbiol. Biotechnol.* **2014**, *98*, 5289–5300. [[CrossRef](#)]
30. Bavykina, A.; Kolobov, N.; Khan, I.S.; Bau, J.A.; Ramirez, A.; Gascon, J. Metal–organic frameworks in heterogeneous catalysis: Recent progress, new trends, and future perspectives. *Chem. Rev.* **2020**, *120*, 8468–8535. [[CrossRef](#)]
31. Loza, K.; Heggen, M.; Epple, M. Synthesis, Structure, Properties, and Applications of Bimetallic Nanoparticles of Noble Metals. *Adv. Funct. Mater.* **2020**, *30*, 1909260. [[CrossRef](#)]
32. Aygun, A.; Gulbagca, F.; Altuner, E.E.; Bekmezci, M.; Gur, T.; Karimi-Maleh, H.; Karimi, F.; Vasseghian, Y.; Sen, F. Highly active PdPt bimetallic nanoparticles synthesized by one-step bioreduction method: Characterizations, anticancer, antibacterial activities and evaluation of their catalytic effect for hydrogen generation. *Int. J. Hydrogen Energy* **2023**, *48*, 6666–6679. [[CrossRef](#)]
33. Jia, Y.P.; Shi, K.; Yang, F.; Liao, J.F.; Han, R.X.; Yuan, L.P.; Hao, Y.; Pan, M.; Xiao, Y.; Qian, Z.Y. Multifunctional nanoparticle loaded injectable thermoresponsive hydrogel as NIR controlled release platform for local photothermal immunotherapy to prevent breast cancer postoperative recurrence and metastases. *Adv. Funct. Mater.* **2020**, *30*, 2001059. [[CrossRef](#)]
34. Agrahari, S.; Singh, A.K.; Gautam, R.K.; Tiwari, I. Answer to comments on: ‘Voltammetric analysis of epinephrine using glassy carbon electrode modified with nanocomposite prepared from Co-Nd bimetallic nanoparticles, alumina nanoparticles and functionalized multiwalled carbon nanotubes’ by Ida Tiwari et al., (Doi: 10.1007/s11356-022-23660-y). *Environ. Sci. Pollut. Res.* **2023**, *30*, 54250–54251. [[CrossRef](#)]
35. Nepal, D.; Kang, S.; Adstedt, K.M.; Kanhaiya, K.; Bockstaller, M.R.; Brinson, L.C.; Buehler, M.J.; Coveney, P.V.; Dayal, K.; El-Awady, J.A. Hierarchically structured bioinspired nanocomposites. *Nat. Mater.* **2023**, *22*, 18–35. [[CrossRef](#)] [[PubMed](#)]
36. Nga, N.; Ngoc, T.; Trinh, N.; Thuoc, T.; Thao, D. Optimization and application of MTT assay in determining density of suspension cells. *Anal. Biochem.* **2020**, *610*, 113937. [[CrossRef](#)] [[PubMed](#)]

37. Ibrahim, N.A.; Hasanin, M.S.; Kamel, S. A new approach for improving the antimicrobial activity of cellulose pulp. *Inorg. Chem. Commun.* **2023**, *155*, 111009. [[CrossRef](#)]
38. Balouiri, M.; Sadiki, M.; Ibnsouda, S.K. Methods for in vitro evaluating antimicrobial activity: A review. *J. Pharm. Anal.* **2016**, *6*, 71–79. [[CrossRef](#)]
39. Noreen, H.; Semmar, N.; Farman, M.; McCullagh, J.S. Measurement of total phenolic content and antioxidant activity of aerial parts of medicinal plant Coronopus didymus. *Asian Pac. J. Trop. Med.* **2017**, *10*, 792–801. [[CrossRef](#)]
40. Panda, J.; Singh, U.P.; Sahu, R. Synthesis, characterization of TiO₂ nano particles for enhancement of electron transport application in DSSC with Cu-BPCA Dye. In Proceedings of the IOP Conference Series: Materials Science and Engineering, Bhubaneswar, India, 21–23 September 2018; p. 012008. [[CrossRef](#)]
41. Gupta, K.; Singh, R.K.P.; Pandey, A.; Pandey, A. Photocatalytic antibacterial performance of TiO₂ and Ag-doped TiO₂ against *S. aureus*, *P. aeruginosa* and *E. coli*. *Beilstein J. Nanotechnol.* **2013**, *4*, 345–351. [[CrossRef](#)]
42. Alosfur, F.K.M.; Ouda, A.A.; Ridha, N.J.; Abud, S.H. Structure and optical properties of TiO₂ nanorods prepared using polyol solvothermal method. *AIP Conf. Proc.* **2019**, *2144*, 030025. [[CrossRef](#)]
43. Zainab; Ahmad, S.; Khan, I.; Saeed, K.; Ahmad, H.; Alam, A.; Almehmadi, M.; Alsaiari, A.A.; Haitao, Y.; Ahmad, M. A study on green synthesis, characterization of chromium oxide nanoparticles and their enzyme inhibitory potential. *Front. Pharmacol.* **2022**, *13*, 1008182. [[CrossRef](#)] [[PubMed](#)]
44. Hou, L.; Feng, K.; Wu, P.; Gao, H. Investigation of water diffusion process in ethyl cellulose-based films by attenuated total reflectance Fourier transform infrared analysis and two-dimensional correlation analysis. *Cellulose* **2014**, *21*, 4009–4017. [[CrossRef](#)]
45. Gençtürk, A.; Kahraman, E.; Güngör, S.; Özsoy, Y.; Sarac, A.S. Effects of polyvinylpyrrolidone and ethyl cellulose in polyurethane electrospun nanofibers on morphology and drug release characteristics. *Turk. J. Pharm. Sci.* **2020**, *17*, 638. [[CrossRef](#)] [[PubMed](#)]
46. Martínez Cortizas, A.; López-Costas, O. Linking structural and compositional changes in archaeological human bone collagen: An FTIR-ATR approach. *Sci. Rep.* **2020**, *10*, 17888. [[CrossRef](#)] [[PubMed](#)]
47. Riaz, T.; Zeeshan, R.; Zarif, F.; Ilyas, K.; Muhammad, N.; Safi, S.Z.; Rahim, A.; Rizvi, S.A.; Rehman, I.U. FTIR analysis of natural and synthetic collagen. *Appl. Anal. Rev.* **2018**, *53*, 703–746. [[CrossRef](#)]
48. Elamin, N.Y.; Indumathi, T.; Ranjith Kumar, E. Pluronic f127 encapsulated titanium dioxide nanoparticles: Evaluation of physicochemical properties for biological applications. *J. Mol. Liq.* **2023**, *379*, 121655. [[CrossRef](#)]
49. Al-hakimi, A.N.; Alminderej, F.; Alhagri, I.A.; Al-Hazmy, S.M.; Farea, M.O.; Abdallah, E.M. Inorganic nanofillers TiO₂ nanoparticles reinforced host polymer polypyrrole for microelectronic devices and high-density energy storage systems. *J. Mater. Sci. Mater. Electron.* **2023**, *34*, 238. [[CrossRef](#)]
50. Rathi, V.H.; Jeice, A.R. Green fabrication of titanium dioxide nanoparticles and their applications in photocatalytic dye degradation and microbial activities. *Chem. Phys. Impact* **2023**, *6*, 100197. [[CrossRef](#)]
51. El-Sayed, S.M.; El-Sayed, H.S.; Youssef, A.M. Facile green preparation of Cr₂O₃ nanoparticles combined with probiotics in hydro-beads to produce integrated yoghurt. *Bioact. Carbohydr. Diet. Fibre* **2023**, *30*, 100354. [[CrossRef](#)]
52. Thakur, T.M.; Lokhande, R.S.; Thigle, M.M.; Patil, V.R. Nanoparticles of chromium oxide by green synthesis using Eucalyptus globulus leaves extract; characterization and biological activity studies. *Mater. Today Proc.* **2023**, *79*, 100–106. [[CrossRef](#)]
53. Parida, P.; Mishra, S.C.; Sahoo, S.; Behera, A.; Nayak, B.P. Development and characterization of ethylcellulose based microsphere for sustained release of nifedipine. *J. Pharm. Anal.* **2016**, *6*, 341–344. [[CrossRef](#)] [[PubMed](#)]
54. Vedhanayagam, M.; Anandasadagopan, S.; Nair, B.U.; Sreeram, K.J. Polymethyl methacrylate (PMMA) grafted collagen scaffold reinforced by PdO–TiO₂ nanocomposites. *Mater. Sci. Eng. C* **2020**, *108*, 110378. [[CrossRef](#)] [[PubMed](#)]
55. Bak, S.Y.; Lee, S.W.; Choi, C.H.; Kim, H.W. Assessment of the influence of acetic acid residue on type I collagen during isolation and characterization. *Materials* **2018**, *11*, 2518. [[CrossRef](#)] [[PubMed](#)]
56. Maheswari, P.; Ponnusamy, S.; Harish, S.; Ganesh, M.R.; Hayakawa, Y. Hydrothermal synthesis of pure and bio modified TiO₂: Characterization, evaluation of antibacterial activity against gram positive and gram negative bacteria and anticancer activity against KB Oral cancer cell line. *Arab. J. Chem.* **2020**, *13*, 3484–3497. [[CrossRef](#)]
57. Mosquera-Vargas, E.; Herrera-Molina, D.; Diosa, J.E. Photocatalytic behavior of TiO₂ and TiO₂/CS nanoparticles under UV irradiation. *Rev. UIS Ing.* **2022**, *21*, 77–84. [[CrossRef](#)]
58. Jafari, A.; Rashidipour, M.; Kamarehi, B.; Alipour, S.; Ghaderpoori, M. Toxicity of green synthesized TiO₂ nanoparticles (TiO₂ NPs) on zebra fish. *Environ. Res.* **2022**, *212*, 113542. [[CrossRef](#)]
59. Alharbi, W. Structural, compositional study, and thermal behavior of TiO₂/Cr₂O₃/GO nanocomposite for methylene blue degradation. *J. Photochem. Photobiol. A Chem.* **2023**, *439*, 114597. [[CrossRef](#)]
60. Yasmeen, G.; Hussain, S.; Tajammal, A.; Mustafa, Z.; Sagir, M.; Shahid, M.; Ibrar, M.; Elqahtani, Z.M.; Iqbal, M. Green synthesis of Cr₂O₃ nanoparticles by Cassia fistula, their electrochemical and antibacterial potential. *Arab. J. Chem.* **2023**, *16*, 104912. [[CrossRef](#)]
61. Su, J.; Xue, H.; Gu, M.; Xia, H.; Pan, F. Synthesis of spherical Cr₂O₃ nanoparticles by a microwave refluxing method and their photocatalytic properties. *Ceram. Int.* **2014**, *40*, 15051–15055. [[CrossRef](#)]
62. Kim, H.-J.; Ferracane, J.L.; Park, M.; Choi, K.-K. Effect of ethyl cellulose coating as an evaluation agent against contamination on the bond strength of zirconia restorations: An in vitro study. *J. Prosthet. Dent.* **2022**, *127*, 766.e1–766.e9. [[CrossRef](#)]
63. Mohd Nasir, N.F.B.; Sahidan, S.I.; Rampado, M.; Raha, M.G.; Kadri, N.A.; Zain, N.M. Characterization of Collagen/PEO 600 K for Tissue Engineering Scaffold. In Proceedings of the 3rd Kuala Lumpur International Conference on Biomedical Engineering 2006, Kuala Lumpur, Malaysia, 11–14 December 2006; Springer: Berlin/Heidelberg, Germany, 2007; pp. 680–683. [[CrossRef](#)]

64. Hasanin, M.; Labeeb, A.M. Dielectric properties of nicotinic acid/methyl cellulose composite via “green” method for anti-static charge applications. *Mater. Sci. Eng. B* **2021**, *263*, 114797. [[CrossRef](#)]
65. Hariharan, D.; Thangamuniandi, P.; Jegatha Christy, A.; Vasantharaja, R.; Selvakumar, P.; Sagadevan, S.; Pugazhendhi, A.; Nehru, L.C. Enhanced photocatalysis and anticancer activity of green hydrothermal synthesized Ag@TiO₂ nanoparticles. *J. Photochem. Photobiol. B Biol.* **2020**, *202*, 111636. [[CrossRef](#)] [[PubMed](#)]
66. Khan, S.A.; Shahid, S.; Hanif, S.; Almoallim, H.S.; Alharbi, S.A.; Sellami, H. Green synthesis of chromium oxide nanoparticles for antibacterial, antioxidant anticancer, and biocompatibility activities. *Int. J. Mol. Sci.* **2021**, *22*, 502. [[CrossRef](#)] [[PubMed](#)]
67. De Dicastro, C.L.; Correa, M.G.; Martínez, F.B.; Streitt, C.; Galotto, M.J. Antimicrobial effect of titanium dioxide nanoparticles. In *Antimicrobial Resistance: A One Health Perspective*; BoD—Books on Demand: Norderstedt, Germany, 2020.
68. Nguyen, T.L.A.; Bhattacharya, D. Antimicrobial Activity of Quercetin: An Approach to Its Mechanistic Principle. *Molecules* **2022**, *27*, 2494. [[CrossRef](#)]
69. Mohammed, H.A.; Al-Omar, M.S.; El-Readi, M.Z.; Alhowail, A.H.; Aldubayan, M.A.; Abdellatif, A.A.H. Formulation of Ethyl Cellulose Microparticles Incorporated Pheophytin A Isolated from *Suaeda vermiculata* for Antioxidant and Cytotoxic Activities. *Molecules* **2019**, *24*, 1501. [[CrossRef](#)] [[PubMed](#)]
70. Nurilmala, M.; Hizbulah, H.H.; Karnia, E.; Kusumaningtyas, E.; Ochiai, Y. Characterization and Antioxidant Activity of Collagen, Gelatin, and the Derived Peptides from Yellowfin Tuna (*Thunnus albacares*) Skin. *Mar. Drugs* **2020**, *18*, 98. [[CrossRef](#)]
71. Santhoshkumar, T.; Rahuman, A.A.; Jayaseelan, C.; Rajakumar, G.; Marimuthu, S.; Kirthi, A.V.; Velayutham, K.; Thomas, J.; Venkatesan, J.; Kim, S.K. Green synthesis of titanium dioxide nanoparticles using Psidium guajava extract and its antibacterial and antioxidant properties. *Asian Pac. J. Trop. Med.* **2014**, *7*, 968–976. [[CrossRef](#)]
72. Shahid, H.; Arooj, I.; Zafar, S.; Saba. Honey-mediated synthesis of Cr₂O₃ nanoparticles and their potent anti-bacterial, anti-oxidant and anti-inflammatory activities. *Arab. J. Chem.* **2023**, *16*, 104544. [[CrossRef](#)]
73. Balyan, S.; Mukherjee, R.; Priyadarshini, A.; Vibhuti, A.; Gupta, A.; Pandey, R.P.; Chang, C.M. Determination of Antioxidants by DPPH Radical Scavenging Activity and Quantitative Phytochemical Analysis of *Ficus religiosa*. *Molecules* **2022**, *27*, 1326. [[CrossRef](#)]

Disclaimer/Publisher’s Note: The statements, opinions and data contained in all publications are solely those of the individual author(s) and contributor(s) and not of MDPI and/or the editor(s). MDPI and/or the editor(s) disclaim responsibility for any injury to people or property resulting from any ideas, methods, instructions or products referred to in the content.